Field Curvature Correction Using Focal Sweep

Shigehiko Matsunaga and Shree K. Nayar

***Abstract*—Camera optics design has become increasingly complex to keep pace with the demand for ever increasing imaging resolution. This complexity results in several disadvantages, including significant increase in size, cost, and weight of the camera. In this paper, we propose methods to simplify the lens of an imaging system without sacrificing resolution. Our approach is to use either the focal stack or the focal sweep method to emulate a curved image sensor. This enables us to design a lens without the need to correct for field curvature. The end result is a lens with significantly lower complexity than a lens that is corrected for field curvature. We have verified the performance and practical viability of our approach using both simulations and experiments with prototype focal stack and focal sweep cameras.**

***Index Terms*—Depth of field, field curvature, focal sweep, imaging optics, programmable pixel exposure, and computational imaging.**

I. Introduction

CONSUMER cameras currently produce photographs with tens of millions of pixels. The demand for higher resolution cameras continues in response to the needs of applications in fields as diverse as photography, medical care, automobile safety, security, factory automation, robotics, etc. The field of camera optics development has correspondingly become increasingly complex as it tries to keep pace with the ever increasing resolution of image sensors. In optics design today, minimizing optical aberrations is the key to achieving high performance.

Optical aberrations are classified as either monochromatic aberration or chromatic aberration [1]. Monochromatic aberration consists of five types: spherical aberration, coma, astigmatism, field curvature, and distortion. These five aberrations are also known as Seidel's aberrations. Chromatic aberration includes two components: longitudinal chromatic aberration and lateral chromatic aberration. Minimizing all seven of the above aberrations can be achieved by combining several lenses. However, using multiple lenses comes with several disadvantages, including a significant increase in the size, cost and weight of the camera. For these reasons, it would be highly beneficial if we could find ways to simplify the lens of an imaging system without sacrificing resolution.

Manuscript received January 18, 2015; revised June 29, 2015; accepted September 29, 2015. Date of publication October 14, 2015; date of current version December 08, 2015. This work was conducted while S. Matsunaga was a Visiting Scholar at the Computer Vision Laboratory at Columbia University. The associate editor coordinating the review of this manuscript and approving it for publication was Prof. Sabine Susstrunk.

S. Matsunaga is with Sony Corporation, Tokyo 108-0075, Japan (e-mail: Shigehiko.Matsunaga@jp.sony.com).

S. K. Nayar is with the Department of Computer Science, Columbia University, New York, NY 10027 USA (e-mail: nayar@cs.columbia.edu).

Color versions of one or more of the figures in this paper are available online at http://ieeexplore.ieee.org.

Digital Object Identifier 10.1109/TCI.2015.2491181

In this paper, we show that focal stack and focal sweep imaging can be utilized to reduce the complexity of a lens. Focal stack and focal sweep are not new concepts [2]–[5] - they are well-known approaches for extending the depth of field (EDOF) of an imaging system and for computing the 3D structure of a scene. Our approach is to use these techniques to correct field curvature instead of using a compound lens. Designing a lens system without correction of field curvature significantly reduces the constraints that need to be invoked during the design process. Our approach is based on the well-known fact that high image quality can be obtained on a curved image surface with a smaller number of lenses. The curved image surface is emulated either by capturing a set of images corresponding to different sensor locations (focal stack) or by capturing a single image with coded exposure while the image sensor is in continuous motion (focal sweep). In addition, color aberration is also reduced by selecting the best focused image surface for each of the color channels.

This paper is organized as follows. First, we describe related work in section 2. Next, in section 3, we discuss ways to design a lens system without correction of field curvature, and describe the advantages of using a curved image surface. In section 4, we propose an algorithm to generate high resolution images by using focal stack and focal sweep to correct field curvature. We have built a focal stack camera and a focal sweep camera using off-the-shelf components to demonstrate our approach. Finally, experimental results that demonstrate the practical feasibility of our approach are shown in section 5.

II. Related Work

A. Array System and Curved Sensor

High resolution images can be captured using a camera array constructed by tiling a large number of cameras [6], [7]. However, such a system is inherently expensive and large. Another approach is to use a multiscale optical system [8], which consists of a large scale objective lens and a small scale non-uniform lens array used to correct aberrations caused by the objective lens. Although the size of a multiscale system can be compact, the individual elements of lens array have different optical aberrations. Such a system can be difficult to manufacture and align with respect to the image sensor. Instead of using the lens array, Ford et al. proposed the use of wave guide coupling of a curved image surface to a conventional (flat) sensor [13]. This solution also must overcome challenges related to alignment and mass manufacturing.

The use of a curved image sensor is one way to correct field curvature and obtain high resolution images. Rim et al. showed that a curved image sensor can decrease the number

of optical elements of a lens without reducing image quality [9]. Cossairt and Nayar proposed a gigapixel imaging system consisting of a ball lens shared by several small planar sensors emulating a curved image surface to acquire high resolution images [10]. Several research groups have attempted to fabricate curved sensors [11], [12]. However, the technology required to mass manufacture curved sensors, especially high resolution ones with high curvature, is not available at this time. In addition, when such technology becomes available, it is expected to be significantly more expensive than the technology used to manufacture today's flat sensors.

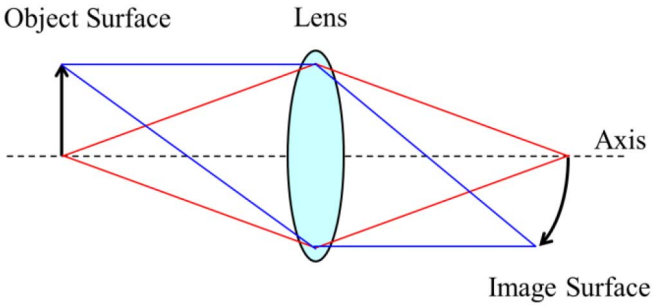

Fig. 1. Field curvature. A fronto-parallel plane is focused on a curved image surface.

B. Focal Stack and Focal Sweep

The combined use of optics and signal processing has been shown to produce various benefits in imaging. Dowski proposed a hybrid optical-signal processing system that uses a phase plate to extend depth of field (DOF) [14]. Robinson showed that spherical aberration can be corrected by signal processing, thus achieving high contrast imaging and EDOF with a simple lens [15]. Cossairt observed that axial chromatic aberrations can be exploited to extend DOF [16].

Other ways to capture an EDOF image are focal stack and focal sweep. Focal stack uses multiple images taken with different focus settings. It has been used for 3D scene reconstruction as well [2], [3]. Focal sweep involves the capture of a single image during a rapid sweep of the sensor, lens or object over a large range of depths. Hausler showed that the DOF of an optical microscope can be extended by moving an object along the optical axis during image exposure [4]. Nagahara extended DOF by moving the sensor instead [5]. In our work, we use the focal stack and focal sweep methods not for extending DOF, but for correcting field curvature, thus enabling us to use a simple lens system for high resolution imaging.

Recently, several works showed that nearly all optical aberrations can be corrected by digital signal processing, and high resolution imaging can be obtained from a simple lens [17], [18]. However, this requires estimation of the point spread function (PSF) which is most often dependent on the depth of scene. Moreover, this approach of image enhancement via PSF deconvolution is prone to an increase in image noise. In our approach, we design the lens to minimize all optical aberrations except for field curvature, which we remove by emulating a curved image sensor using focal stack or focal sweep. We show that this approach achieves high image resolution and high signal-to-noise ratio (SNR) while significantly reducing lens complexity.

III. Lens Design Without Correction of Field Curvature

A. Field Curvature

In an ideal lens, the light from a point light source on the object side would converge at a single point on the image side. Unfortunately, such an ideal lens does not exist. The point light source is instead blurred by optical aberrations resulting from the shape of the lens. As we described in section 1, optical aberrations are classified into seven types. In conventional lens design, all these aberrations are simultaneously minimized by combining several lenses. In this approach, however, as the required resolution of a camera increases, lens design becomes more complex and difficult. In addition, as the required resolution increases, so do the size, cost and weight of the lens. Therefore, it is highly desirable to find a way to simplify a lens system without sacrificing its resolution. In order to simplify the system, we focus on field curvature.

Field curvature is an optical aberration that converts a fronto-parallel planar surface into a curved image surface, as shown in Fig. 1. It is well known that if all other aberrations are absent, a flat image surface can be obtained by reducing the Petzval Sum [19]. If an optical-system contains several widely separated thin elements, the Petzval Sum is given by:

$$P = \sum_{i=1}^{k} 1/n_i f_i, \tag{1}$$

where k is the number of elements, f_i is the focal length of each element, and n_i is the refractive index of each element. The above equation reveals that lenses with both positive and negative focal lengths are necessary to reduce the Petzval Sum. This fact causes lens systems to quickly becomes complex. If we can emulate a curved image surface, we do not need extra lenses to correct field curvature.

B. Triplet Lens Design: With and Without Field Curvature Correction

In this section, we describe the difference between conventional lens design and lens design without correction of field curvature by using the case of a triplet lens. Fig. 2 compares triplet lenses with and without correction of field curvature. All the triplet lenses have the same specification, Fno $= 2.0$, focal length $= 17.6$ mm, and image height $=$ 3.6 mm for a $1/2.5''$ sensor. The lens prescription data is shown in Table I. The optical designs and their performances were generated using the CodeV optical design software [20]. We used a weighted sum of the response at the wavelengths $\lambda = 656.3$ nm, 587.6 nm, 546.1 nm, 486.1 nm, and 435.8 nm, with relative weights of 1, 2, 4, 2, and 1, respectively.

System (a) shows a triplet lens developed using conventional lens design. System (b) shows a triplet lens with a flat image surface, but without correction of field curvature. System (c)

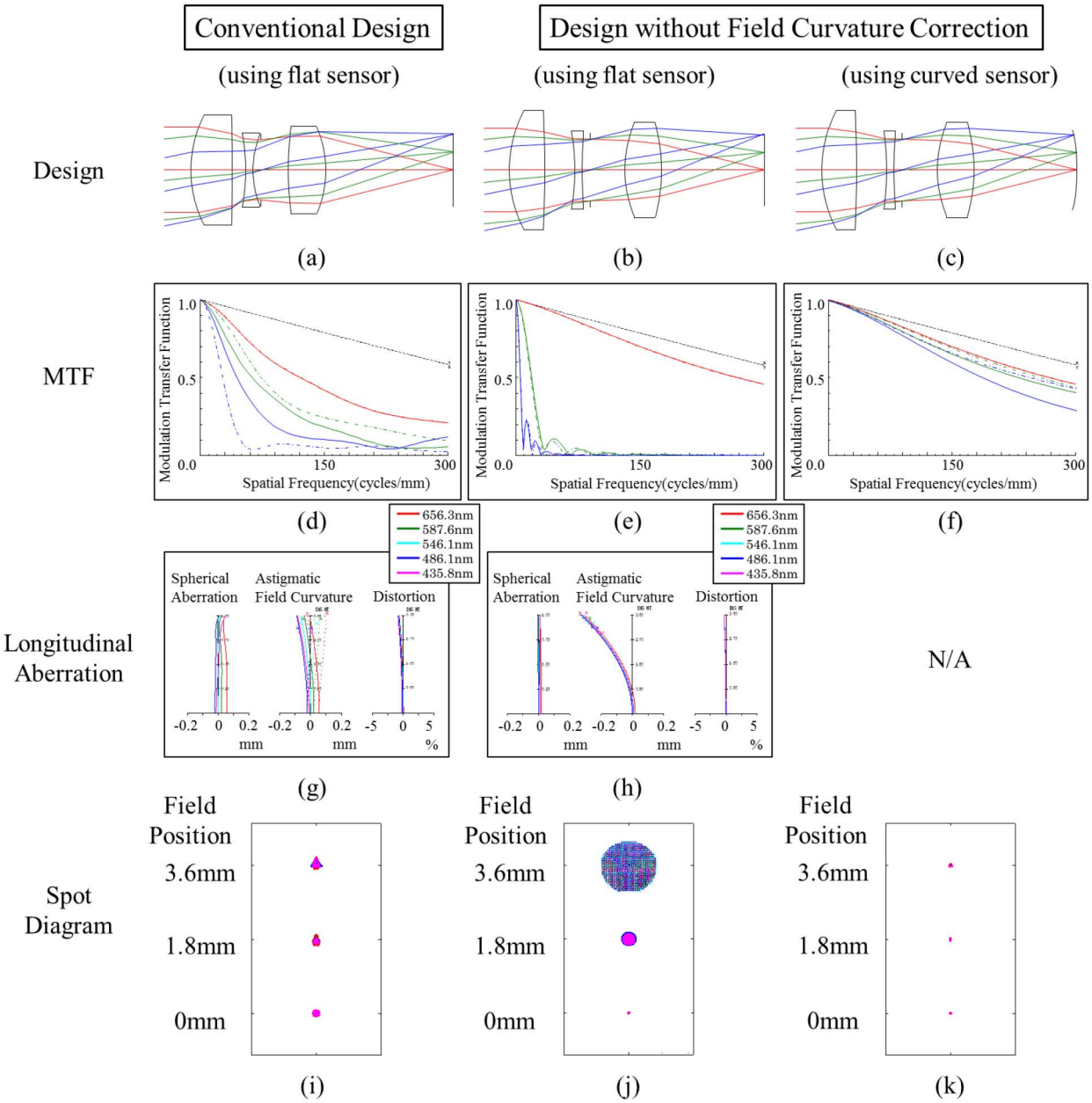

Fig. 2. Comparison of triplet lens implementations. The left column (a, d, g, i) shows the properties of a conventional design triplet lens using a flat sensor. Center column (b, e, h, j) shows the properties of a triplet lens using a flat sensor without correction of field curvature. The right column (c, f, k) shows the properties of the same triplet lens as in the center column, but using a curved sensor instead of a flat one. Relaxing the constraint of field curvature correction and using a curved sensor makes it possible to obtain a high quality image with fewer lenses.

shows the same lens system as in (b), but with a curved image surface. Fig. 2 (d)-(f) show the modulation transfer functions (MTF) of three systems. The diffraction limit (black dotted line), MTF on the axis (red line), MTF for the image heights of 1.8 mm (green line), and 3.6 mm (blue line) are shown. We also show the tangential MTF (solid line) and radial MTF (dashed line). In addition, Fig. 2 (g)-(h) show longitudinal aberration plots and Fig. 2 (i)-(k) show spot diagrams. The different colors of the plots correspond to the five different wavelengths used in the simulation.

First, we compare system (a) with (b). Fig. 2 (g), (i) show that the triplet lens is not sufficient for correcting all the aberrations. Since other aberrations, such as chromatic aberration and astigmatism, are not reduced in exchange for field curvature correction, the MTF for each image height is low [Fig. 2(d)]. On the other hand, Fig. 2(h) shows that other aberrations can be corrected by relaxing the constraint of field curvature correction. It is clear that the off-axis performance is low because of field curvature [Fig. 2(e), (j)]. However, the on-axis MTF is much higher than in the case of system (a). Were the image surface a curved one with a shape consistent with the field curvature [Fig. 2 (c)], the off-axis performance would be as high as that of the on-axis one [Fig. 2(f), (k)]. Therefore, high performance is easily obtained with a curved image surface. In other words, for any desired performance target, a curved image surface simplifies the lens.

TABLE I
THE LENS PRESCRIPTION DATA

Conventional Design

Surface:	Type	Radius	Thickness	nd	vd
1	Standard	11.71	4.24	2.001	29.13
2	Standard	-175	1.34		
3	Standard	-18.3	0.75	2.00272	19.32
4	Standard	9.81	0.8		
STOP	Standard	∞	2.75		
6	Even Asphere	29.93	3.75	1.8208	42.71
7	Even Asphere	-11.18	12.91		

Aspherical Data		k	a	b	c
6	Even Asphere	0	-1.392E-04	-3.706E-07	-2.621E-09
7	Even Asphere	0	1.407E-04	-8.500E-07	0

Design without Field Curvature Correction

Surface:	Type	Radius	Thickness	nd	vd
1	Standard	13	3.57	1.618	63.4
2	Standard	-143.5	3.09		
3	Standard	-23.62	0.75	2.001	29.13
4	Standard	60.95	0.8		
STOP	Standard	∞	3.58		
6	Even Asphere	11.5	3.75	1.4971	81.56
7	Even Asphere	-15.88	10.49		

Aspherical Data		k	a	b	c
6	Even Asphere	0	-1.404E-04	2.130E-06	-8.171E-08
7	Even Asphere	0	-1.365E-08	-7.621E-07	0

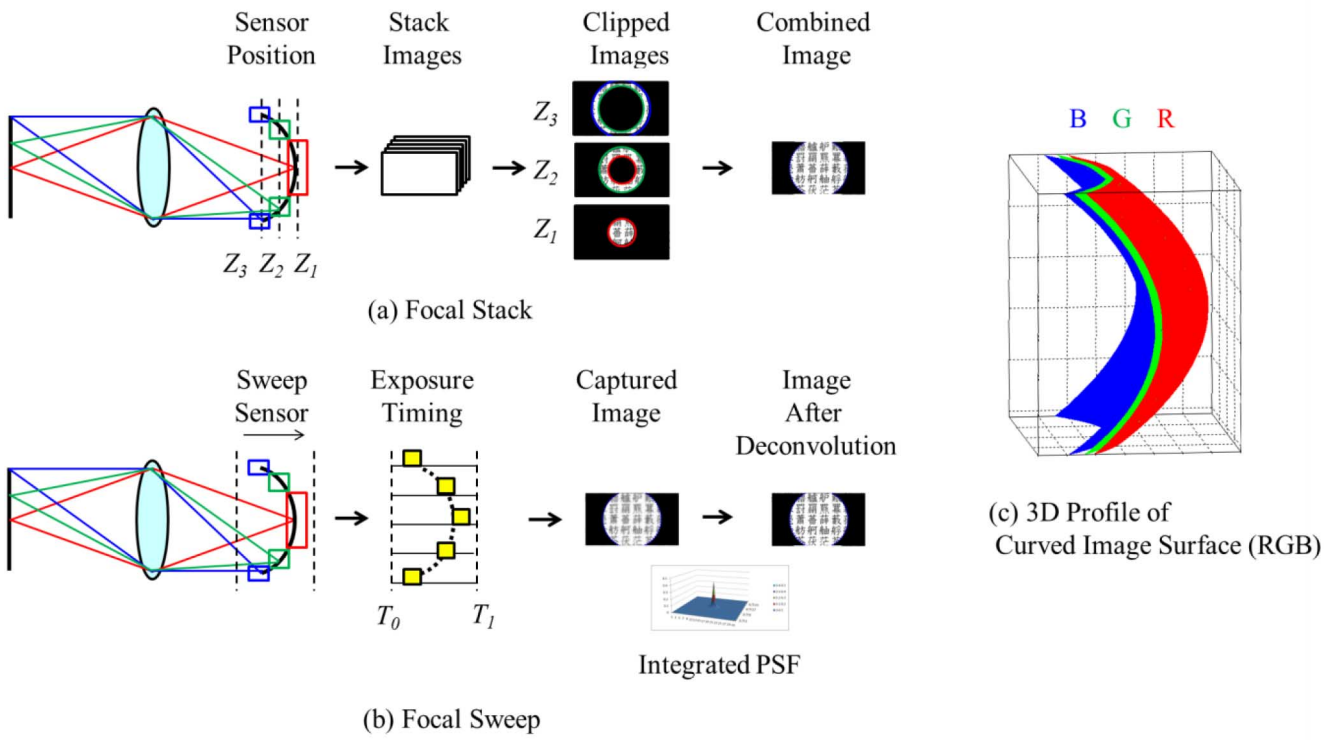

Fig. 3. Flow diagram of the proposed system. (a) Focal stack, (b) focal sweep, and (c) 3D profile of curved image surface (RGB) when chromatic aberration exists. Focal stack and focal sweep are utilized to emulate a curved sensor.

IV. METHOD FOR CAPTURING A HIGH RESOLUTION IMAGE

A. Focal Stack and Focal Sweep for Correction of Field Curvature

Both focal stack and focal sweep can be used to emulate a curved image sensor. Between the two, focal sweep would be the preferred approach as it is fast and requires the capture of a single image. However, it does require the use of an image sensor that has pixel-level exposure control. Therefore, in applications where speed of capture is not critical, focal stack would be a better choice as it can be easily implemented using off-the-shelf components. Fig. 3 illustrates the two approaches. In the case of focal stack [Fig. 3(a)], the images are captured using a set of sensor positions that cover the range of the field curvature. If there are magnification changes and image shifts between images in the stack, they can be corrected by using an off-line calibration of the system. Next, the circular focused area (either a disc or a ring) in each image is clipped from it. By combining the clipped images, we can obtain a single all-focused image. In the case of focal sweep [Fig. 3(b)], a single image is captured while the sensor sweeps the range of field curvature. The exposure timing of each pixel is synchronized with the sensor motion in order to extract the brightness value

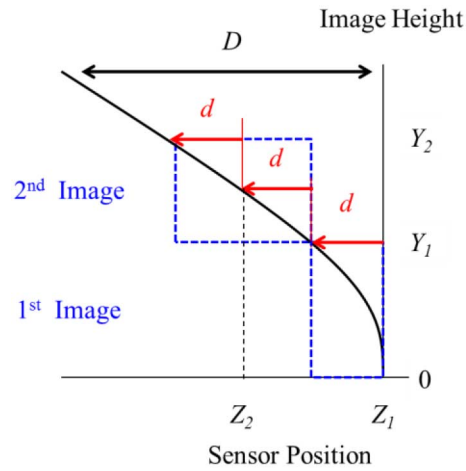

Fig. 4. Optimizing the number of focal stack images. The circular area clipped from each image is determined by the distance d.

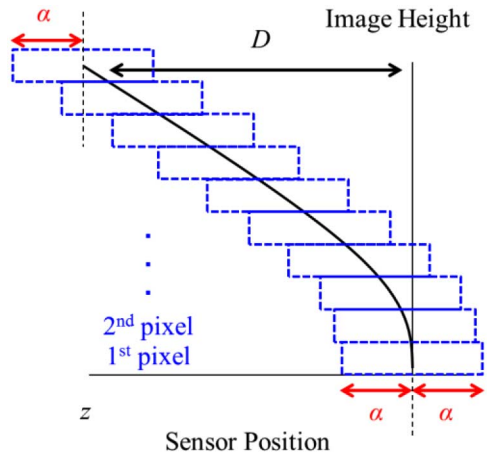

Fig. 5. Focal sweep for covering the whole range of field curvature. The sweep range of each pixel includes the sensor position for which the image is best focused.

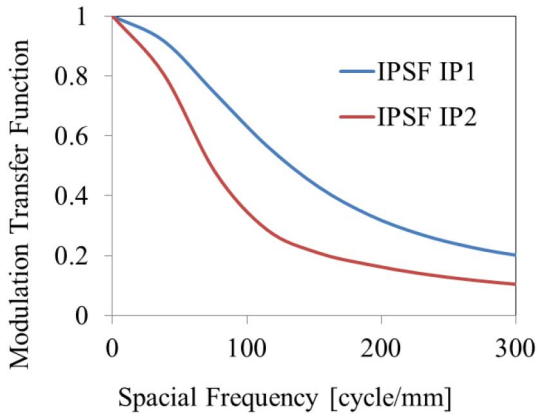

Fig. 6. MTF calculated from IPSF. Sweep range of IP_1 is half of that of IP_2. Sweeping a longer range causes degradation of MTF.

that corresponds when the pixel passes through the curved image surface. Although the captured image is slightly blurred because of motion and the finite exposure time, it can be deblurred by deconvolution with the integrated point spread function (IPSF) (see [5]). Fig. 3(c) shows a 3D surface of a curved image surface for each of the three color channels of the image sensor. The three image surfaces do not coincide since the lens system has chromatic aberration. Although the best focused surface for any given image height is different for each color, our approach can remove chromatic aberration effects as well by clipping (in the case of a stack) and exposing (in the case of sweep) the appropriate pixels for each color. In short, by using focal stack or focal sweep, we are able to remove both field curvature and chromatic aberration by simultaneously emulating curved image surfaces for each of the three color channels of the image sensor. In the case of multispectral imaging, a larger number of curved image surfaces may be emulated, simultaneously.

B. Optimizing the Number of Focal Stack Images

In order to minimize the total exposure time needed to capture the stack images, we optimize the number of images. Our approach is based on the degradation of MTF. This is necessary because a combined image would not be useful if the MTFs of the individual clipped areas are very different. First, we choose a specific spatial frequency fs that we would like to preserve in the final image. We then set a limit q to the permissible degradation of the MTF within the first clipped circular region (from image height 0 to Y_1).

Fig. 4 shows how to divide the whole range of field curvature D. Let us suppose that the image sensor is placed at the position Z_1 where the MTF on the axis is maximized. Then, the MTF at the image height Y_1 is lower than MTF on the axis. If the degradation of MTF is within q, Y_1 becomes the boundary of the circular region clipped from the first image. Then, the distance d is calculated by using a polynomial approximation of the field curvature. The second image is captured when the image sensor is placed at the position Z_2. It is $2d$ away from Z_1. The boundary of the second image Y_2 is also calculated using the polynomial field curvature model. In this way, we determine the boundaries of images, and the total number of images N can be determined as $1 + [D + 2d]$.

C. Integrated PSF for Focal Sweep

In the case of focal sweep, we need to use a finite exposure time for each pixel to ensure that the captured image is bright enough. This corresponds to a finite sweep range for each pixel, which affects the MTF of the Integrated PSF. Fig. 5 illustrates how the whole range of the field curvature can be covered. The sweep range of each pixel is 2α and it includes the sensor position (black curve) for which the image is best focused.

Let $P(x, y, z)$ denote the PSF when the object plane and the image height of sensor are fixed. The Integrated PSF (IPSF) is given by

$$IPSF = \int_{z_0-\alpha}^{z_0+\alpha} P(x, y, z)\, dz, \tag{2}$$

where z_0 is the sensor position for which the image is best focused, and α is half of the sweep range along the z axis.

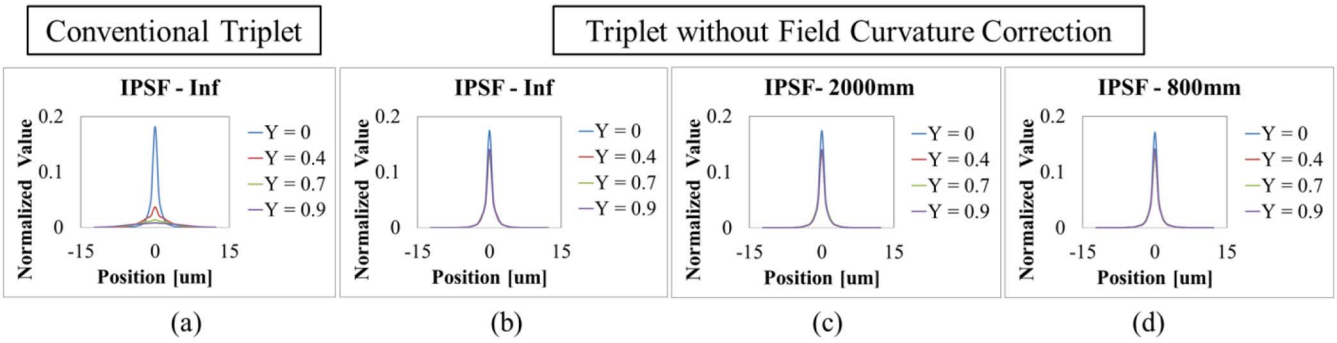

Fig. 7. The simulated IPSF for different settings. Compared with the IPSF of a conventional triplet lens, the IPSF of a triplet without correction of field curvature does not vary with the normalized image height and the object distance.

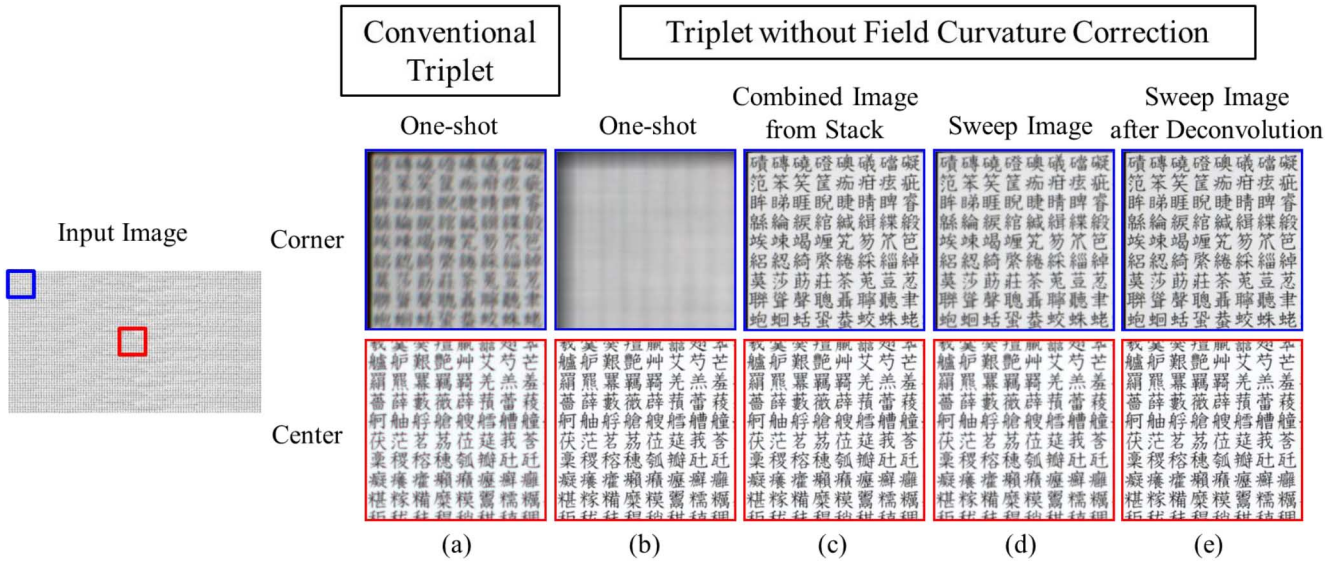

Fig. 8. Simulation results for field curvature correction using focal stack and focal sweep. (a) One-shot image using a conventional triplet lens, (b) one-shot image using a triplet lens without correction of field curvature, (c) focal stack image obtained by combining circular regions of the stack images, (d) focal sweep image emulated by combining multiple images, and (e) focal sweep image after deconvolution with the IPSF. Note that image quality in the corner areas is significantly improved using focal stack and focal sweep.

Fig. 6 shows the MTF calculated from the IPSF of the triplet lens without correction of field curvature [Fig. 2(b)]. We used the Zemax optical design software to calculate the IPSF from the discrete PSF, instead of integration of the continuous PSF. Matlab was used to calculate the MTF from the IPSF [21], [22]. The MTF of IP_1 is obtained using $\alpha = 20$ um, while the MTF of IP_2 is obtained using $\alpha = 40$ um. Image height is on-axis in both cases. As can be seen, the MTF calculated from the IPSF is affected by α. A large value of α (e.g., IP_2) causes degradation of the MTF. These plots also indicate that, as α increases, noise would be more highly amplified after deconvolution. On the other hand, α also affects the total exposure time. When exposure time of each pixel while sweeping is t_s, the constant velocity of sweep is given by $v_s = 2\alpha/t_s$. Then, the total exposure time T can be determined as:

$$\begin{aligned} T &= (D + 2\alpha)/v_s, \\ &= \left(\frac{D}{2\alpha} + 1\right) * t_s. \end{aligned} \tag{3}$$

The above expression shows that as α increases, T decreases for any given t_s. In short, there is a trade-off between noise in the final image and the total exposure time used.

Another feature of our approach is that the IPSF does not vary significantly with image height and object distance. Fig. 7(a) shows the 1D profile of the IPSF calculated using the conventional triplet design [Fig. 2(a)]. Fig. 7(b)-(d) show the 1D profiles of the IPSF calculated using the triplet lens without correction of field curvature [Fig. 2(b)], for different object distances, when $\alpha = 20$ um, and normalized image height Y varies from 0 to 0.9. As seen in Fig. 7(a), the IPSF of the conventional triplet varies significantly with image height. In contrast, the IPSF of the triplet without correction of field curvature does not vary with respect to normalized image height and the object distance. Therefore, we are able to use a single IPSF for recovering the final high resolution image via deconvolution.

D. Simulation Results

To verify our concept, we use the 2D image simulation tool, CodeV [20]. We choose $fs = 80$ cycle/mm, and $q = 0.05$ for

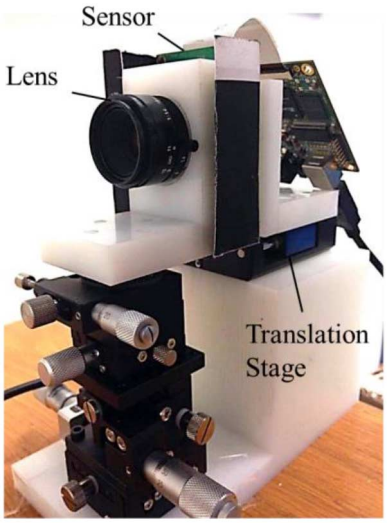

Focal Stack Camera

Fig. 9. Focal stack camera. The system includes a sensor whose position is controlled by a translation stage.

(a) Commercial Lens (b) Doublet

Fig. 10. Lens Simplification. (a) A commercial lens (with five elements), and (b) a simplified lens (with two elements) that produces similar image quality when used with a focal stack or focal sweep.

our simulations. This gives us the following parameter values: $D = 332$ um, $d = 4$ um, and $N = 42$. Fig. 8 shows a comparison between a single image produced by a conventional triplet (a), a single image produced by a triplet without correction of field curvature (b), and a combined image which is computed from a focal stack (c). The size of each Kanji character in the images is about 44×44 pixels and the size of the images is 3840×2160 pixels. As expected, the combined image looks sharper than the other two, especially in the corners. Although the system uses a camera lens with only three elements, its quality is equivalent to that of a 4K resolution camera lens.

For our focal sweep simulation, we simulated a large number of images corresponding to different sensor positions and used them to obtain the focal sweep image. Fig. 8(d) shows the focal sweep image consisting of 42 circular sections. Each circular section is computed by averaging the focused image and four of its neighbor images within the range of $\pm\alpha$, when $\alpha = 20$ um. Although it is a little blurred compared with (c), it still looks sharper than (a), and (b). Moreover, the focal sweep image can be easily deblurred by deconvolution. A number of techniques have been proposed for deconvolution [23]. We used Wiener deconvolution with the single IPSF shown in Fig. 7(b), where $Y = 0$, to obtain the result shown in (e).

V. Experiments

A. Focal Stack

We first built the focal stack camera shown in Fig. 9. It consists of a lens, an image sensor that has a rolling shutter (Lumenera, Lw570c, $1/2.5''$ CMOS sensor with 2592×1944 pixels), and a translation stage (Physik Instrumente, M-111.1DG). This setting is almost the same as the one used in previous work on extended depth of field [5]. We used a compact commercial lens with 16 mm focal length and Fno $= 5.6$ (Edmund Optics, #56-528). For the simplified lens, we used an aspherized doublet lens with 14 mm focal length and Fno $= 5$ (Edmund Optics, #49-658). Fig. 10 shows a side-by-side comparison between the two lenses. The commercial lens uses five elements to correct all the aberrations including field curvature, while the doublet consists of only two elements, which are insufficient to correct for all the aberrations. Thus field curvature is not corrected.

Fig. 11 shows a comparison between images captured using the two lenses. Due to the slight difference in the fields of view of the two lenses, we use posters of different sizes as targets for capturing the images. Fig. 11(a) shows an image captured by the commercial lens with an exposure time of 25 ms. The resolution in the corners is high because the field curvature is well-corrected by the five elements of the lens. Fig. 11(b) shows a one-shot image focused at the center with an exposure time of 20 ms. The corner of the image is severely blurred due to field curvature. Fig. 11(c) shows a focal stack image consisting of 30 circular images regions where the regions are calculated using simulation with $fs = 60$ cycle/mm, $q = 0.05$, $D = 468$ um, and $d = 16$ um. The total exposure time was 600 ms for measuring the 30 circular images. The image quality in the corners is significantly improved compared with (b).

While capturing a focal stack, the motion of the sensor causes changes in magnification and introduces shifts in the stack of images. These effects are measured once with a calibration chart and then corrected when each subsequent stack is captured. In addition, field curvature in an actual lens varies from simulated data. In order to select the best-focused pixels from stack images, we apply the algorithm for determining depth from focus shown in Fig. 12. As our first test target, we use a textured Kanji chart. After capturing a focal stack, magnification change and image shift are corrected using the calibration data. Then, we apply a modified Laplacian filter to the stack images in order to obtain a focus index map, which represents the best-focused image number for each pixel [3]. Since the focus index map is not smooth, a polynomial is fitted to it to

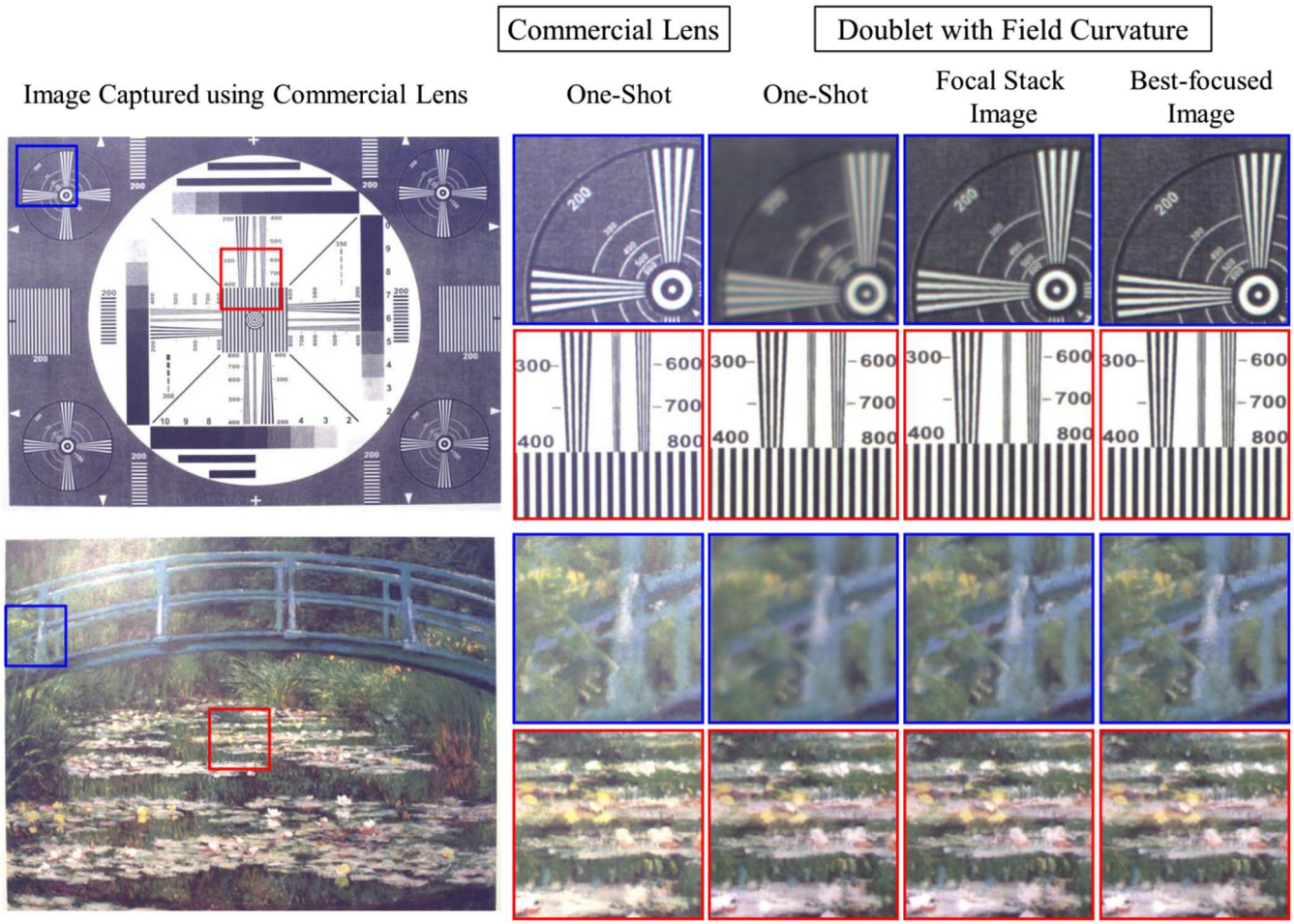

Fig. 11. Comparison of images captured using a commercial lens and a doublet. (a) One-shot image taken using a commercial lens, (b) one-shot image taken using the doublet without correction of field curvature, (c) focal stack image consisting of circular image regions using simulated lens data, (d) focal stack image consisting of best-focused pixels computed using a depth of focus algorithm. The focal stack image has almost the same image quality as the one-shot image captured by the commercial lens. Moreover, selecting best-focused pixels from the focal stack results in higher image quality.

make the map smooth. By selecting the best focused pixels from stack images using this smoothed index map, the image quality in the corners is further improved as seen in Fig. 11(d). In our experiments, we used only a single index map corresponding to the green channel of color image. If a lens has noticeable chromatic aberrations, an index map can be used for each of the three color channels to correct for the chromatic aberrations, as shown in Fig. 12.

B. Focal Sweep

In our context, the use of focal sweep requires the use of an image sensor with per-pixel exposure timing control. Such a sensor is not available at this point in time. Therefore, we emulate it by using a liquid crystal on silicon (LCoS) device. LCoS has been used as a spatial light modulator in various imaging applications [24], [25]. Our focal sweep camera design is similar to the one used in these previous works.

Fig. 13 shows our focal sweep camera system. It consists of an objective lens, a field lens, three relay lenses, a polarizing beam splitter, an LCoS device, an image sensor, and a translation stage. Only off-the-shelf components are used in the system. We used an aspherized doublet lens with 14 mm focal length and Fno $= 5$ as the objective lens (Edmund Optics, #49-658), two plano-convex lenses with 30 mm focal length as the field lens (Edmund Optics, #45-363), an achromatic doublet lens with 100 mm focal length as the relay lens (Edmund Optics, #32-327), a polarizing cube beam splitter (Edmund Optics, #49-002), an LCoS device (Forth Dimension Displays, SXGA-3DA, resolution 1280×1024), an image sensor with a global shutter (Lumenera, Lw230c, $1/1.8''$ CCD with 1616×1216 pixels), and a translation stage (Physik Instrumente, M-111.1DG). Captured images are of size 1280×960 pixels.

As shown in Fig. 13(a), incident light from the scene is focused on the virtual image plane by the objective lens. The field lens is used to prevent vignetting. The beam splitter separates the light into S-polarized light and P-polarized light by reflection and transmission, respectively. The transmitted P-polarized light is reflected by the LCoS device. The LCoS device can rotate the polarization direction at each pixel based on the binary data applied to it. If the pixel value is 1, the P-polarized light is converted into S-polarized light. S-polarized light is again reflected by the beam splitter, and reaches the image sensor. Conversely, if the pixel value is 0, P-polarized

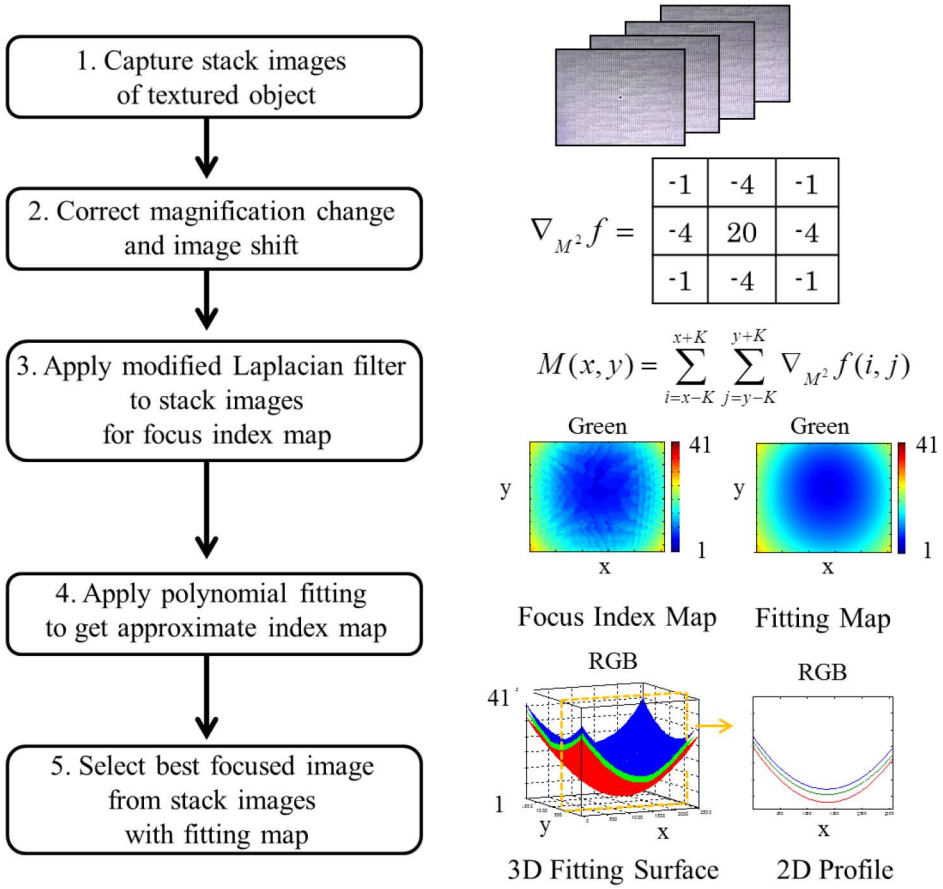

Fig. 12. Algorithm for depth of focus. Best focused pixels are selected using a focus index map obtained by applying a focus operator to the focal stack.

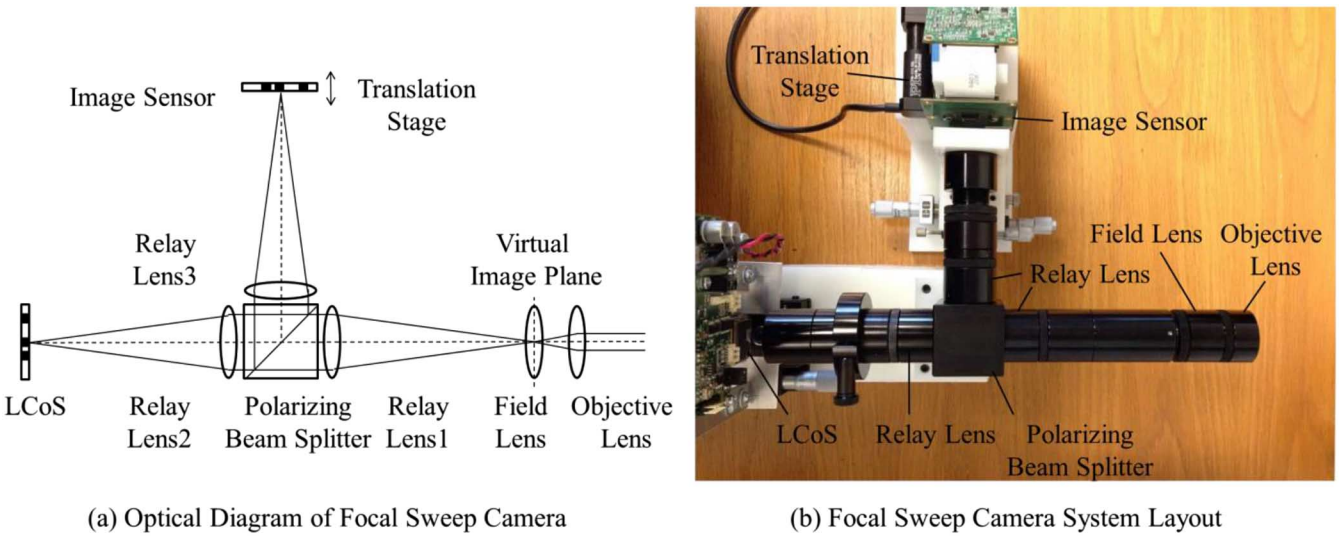

Fig. 13. Focal sweep camera. (a) Optical diagram of the focal sweep camera, and (b) the implemented focal sweep camera system. The focal sweep camera emulates per-pixel exposure by using a liquid crystal on silicon (LCoS) device.

light is reflected with the same polarization direction. Then, it is blocked by the beam splitter. In this way, we can emulate per-pixel exposure control. The camera, LCoS, and translation stage are synchronized by using a trigger signal from a function generator. Our system is limited in terms of exposure time owing to the use of the LCoS device. It cannot display the same binary image for more than 20 ms, and it also needs to display the complementary binary image for the same period immediately after. Due to this limitation, we captured our set of circular images by using a sensor sweep for each one of the images. The final focal sweep image is thus a combination of these circular focal sweep images, and is equivalent to a single

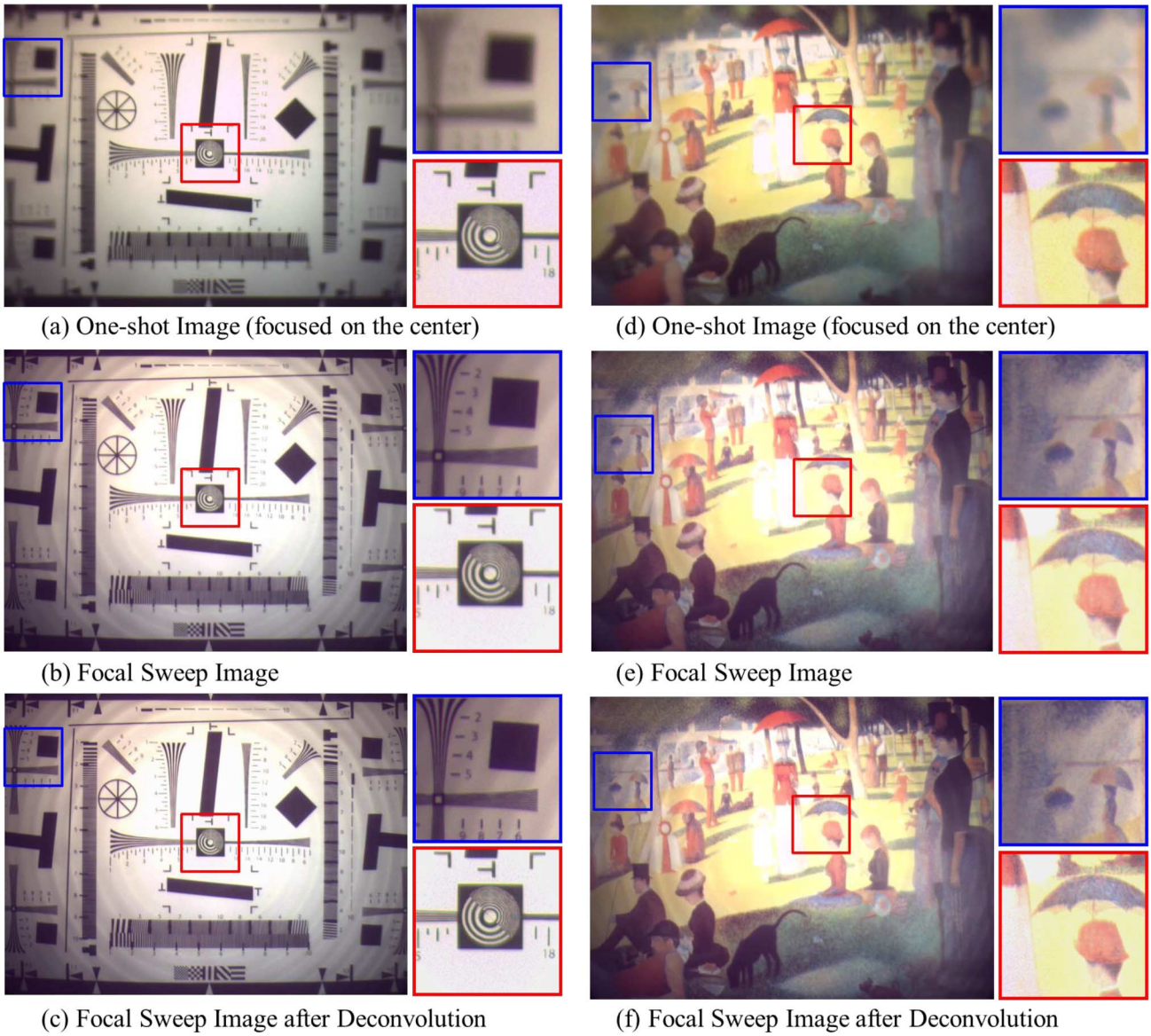

Fig. 14. Examples of focal sweep images. (a), (d) One-shot image captured using a doublet with the focus maximized for the center of the image. (b), (e) Focal sweep image obtained by combining 13 circular images. (c), (f) Focal sweep image after applying deconvolution. Resolution in the corner regions is significantly improved by our approach.

focal sweep image captured using a single sweep using a system without the above timing constraints.

Our focal sweep images are 1280×960 pixels in size. Fig. 14(a), (d) show one-shot images focused at the center with an exposure time of 16 ms. Clearly, the surrounding area of the image is strongly blurred due to field curvature. Fig. 14(b), (e) show a focal sweep image consisting of 13 circular sections. Each circular section is captured using a sweep range of 24 um with an exposure time of 16 ms, resulting in a total exposure time of 208 ms. The translation stage moves at a speed of 1.5 mm/s during the exposure time. As expected, the resolution away from the center is significantly improved for both scenes. Though the center area is slightly blurred due to the sweep, it can be deblurred by using deconvolution. Fig. 14(c), (f) show the result of deblurring using Wiener deconvolution with a single IPSF that is optimized for the center of the image. Note that the images have ring-shaped artifacts. This is the result of light leakage caused by the use of the LCoS. This artifact would not appear when a sensor with per-pixel exposure control is used.

VI. Conclusion

In this paper, we showed that by relaxing the constraint of correcting field curvature and using a curved image sensor, we can significantly simplify the lens system without compromising image resolution. We proposed the use of focal stack and focal sweep to emulate a curved image sensor. In addition, we implemented focal stack and focal sweep cameras using off-the-shelf components, and demonstrated the effectiveness of our approach via experiments. We showed that by using the focal stack method a doublet lens having field curvature can

capture an image with the same resolution as a commercial lens consisting of five elements. We emulated a curved image sensor using focal sweep by using an LCoS device that enables per-pixel exposure control. With this system we showed that a high resolution image can be acquired with a simple lens system.

While our proposed approach can be used in various scenarios, it is not suitable for imaging fast moving objects. This limitation is akin to the one faced by rolling shutter sensors. In our case, the pixels have different exposure timings based on their radial distance from the image center.

REFERENCES

[1] W. Smith, *Modern Optical Engineering: The Design of Optical Systems*, 4th ed. New York, NY, USA: McGraw-Hill, 2008.

[2] T. Darrel and K. Wohn, "Pyramid based depth from focus," in *Proc. IEEE Conf. Comput. Vis. Pattern Recog.*, 1988, pp. 504–509.

[3] S. Nayar and Y. Nakagawa, "Shape from focus," *IEEE Trans. Pattern Mach. Intell.*, vol. 16 no. 8, pp. 824–831, 1994.

[4] G. Häusler, "A method to increase the depth of focus by two step image processing," *Opt. Commun.*, vol. 6, no. 1, pp. 38–42, 1972.

[5] H. Nagahara, S. Kuthirummal, C. Zhou, and S. Nayar, "Flexible depth of field photography," in *Proc. Eur. Conf. Comput. Vis.*, 2008, pp. 60–73.

[6] B. Wilburn *et al.*, "High performance imaging using large camera arrays," *ACM Trans. Graph. (TOG)*, vol. 24, no. 3, pp. 765–776, 2005.

[7] Y. Nomura, L. Zhang, and S. Nayar, "Scene collages and flexible camera arrays," in *Proc. 18th Eurograph. Conf. Render. Techn.*, 2007, pp. 127–138.

[8] D. Brady and N. Hagan, "Multiscale lens design," *Opt. Express*, vol. 17, no. 13, pp. 10659–10674, 2009.

[9] S. Rim, P. Catrysee, R. Dinyari, K. Huang, and P. Peumans, "The optical advantages of curved focal plane arrays," *Opt. Express*, vol. 16, no. 7, pp. 4965–4971, 2008.

[10] O. Cossairt, D. Miau, and S. Nayar, "Gigapixel computational imaging," in *Proc. IEEE Conf. Comput. Photogr.*, 2011, pp. 1–8.

[11] R. Dinyari, S. Rim, K. Huang, P. Catrysee, and P. Peumans, "Curving monolithic silicon for nonplanar focal plane array applications," *Appl. Phys. Lett.*, vol. 92, p. 091114, 2008.

[12] H. Ko *et al.*, "A hemispherical electronic eye camera based on compressible silicon optoelectronics," *Nature*, vol. 454, pp. 748–753, 2008.

[13] J. Ford *et al.*, "Fiber-coupled monocentric lens imaging," in *Imaging and Applied Optics OSA Technical Digest*, Washington, DC, USA: Optical Society of America, 2013, paper CW4C.2 [Online]. Available: https://www.osapublishing.org/abstract.cfm?uri=COSI-2013-CW4C.2

[14] E. Dowski Jr. and W. Cathey, "Extended depth of field through wave-front coding," *Appl. Opt.*, vol. 34, no. 11, pp. 1859–1866, 1995.

[15] M. Robinson, G. Feng, and D. Stork, "Spherical coded imagers: Improving lens speed, depth-of-field, and manufacturing yield through enhanced spherical aberration and compensating image processing," *Proc. SPIE*, vol. 7429, p. 74290M, 2009.

[16] O. Cossairt and S. Nayar, "Spectral focal sweep: Extended depth of field from chromatic aberrations," in *Proc. IEEE Conf. Comput. Photogr.*, 2010, pp. 1–8.

[17] C. Schuler, M. Hirsch, S. Harmeling, and B. Schölkopf, "Non-stationary correction of optical aberrations," in *Proc. IEEE Conf. Comput. Vis.*, 2011, pp. 659–666.

[18] F. Heide, M. Rouf, and M. Hullin, "High-quality computational imaging through simple lenses," *ACM Trans. Graph. (TOG)*, vol. 32, no. 5, article 149, 2013 [Online]. Available: http://dl.acm.org/citation.cfm?id=2516974

[19] R. Kingslake and R. Johnson, *Lens Design Fundamentals*, 2nd ed. Bellingham, WA, USA: SPIE, 2009.

[20] MathWorks, Inc. *CodeV Optical Design Software* [Online]. Available: http://www.mathworks.com/

[21] Zemax, LLC.*Zemax Optical Design Software* [Online]. Available: https://www.zemax.com/home

[22] Synopsys, Inc.*Maltab* [Online]. Available: http://optics.synopsys.com/

[23] P. Jansson, *Deconvolution of Images and Spectra*. New York, NY, USA: Academic, 1996.

[24] H. Nagahara, C. Zhou, T. Watanabe, H. Ishiguro, and S. Nayar, "Programmable aperture camera using LCoS," in *Proc. 11th Eur. Conf. Comput. Vis.*, 2010, pp. 337–350.

[25] Y. Hitomi, J. Gu, M. Gupta, T. Mitsunaga, and S. Nayar, "Video from a single coded exposure photograph using a learned over-complete dictionary," in *Proc. Int. Conf. Comput. Vis.*, 2011, pp. 287–294.

Shigehiko Matsunaga received the B.Eng. and M.Eng. degrees in electrical engineering from Osaka University, Osaka, Japan, in 2003 and 2005, respectively. He has been working with Sony Corporation, Tokyo, Japan, since 2005. He was a Visiting Scholar at Columbia University from 2013 to 2014. His research interests include optical lens design and computational imaging.

Shree K. Nayar received the Ph.D. degree in electrical and computer engineering from the Robotics Institute, Carnegie Mellon University, Pittsburgh, PA, USA. He is the T. C. Chang Professor of Computer Science with Columbia University, New York, NY, USA. He is the Head of the Columbia Vision Laboratory (CAVE), which develops advanced computer vision systems. His research is focused on three areas—the creation of novel cameras that provide new forms of visual information, the design of physics based models for vision and graphics, and the development of algorithms for understanding scenes from images. His research interests include applications in the fields of digital imaging, computer graphics, and robotics and human-computer interfaces. For his contributions to computer vision and computational imaging, he was elected to the National Academy of Engineering in 2008, the American Academy of Arts and Sciences in 2011, and the National Academy of Inventors in 2014. He was the recipient of the David Marr Prize (1990 and 1995), the David and Lucile Packard Fellowship (1992), the National Young Investigator Award (1993), the NTT Distinguished Scientific Achievement Award (1994), the Keck Foundation Award for Excellence in Teaching (1995), the Columbia Great Teacher Award (2006), and the Carnegie Mellon Alumni Achievement Award (2009).